



ELSEVIER

Contents lists available at ScienceDirect

Electrochimica Acta

journal homepage: www.elsevier.com/locate/electacta

The anodic formation of sulfide and oxide films on copper in borate-buffered aqueous chloride solutions containing sulfide

M. Guo^a, J. Chen^{a,*}, C. Lilja^b, V. Dehnavi^c, M. Behazin^d, J.J. Noël^{a,c,*}, D.W. Shoesmith^{a,c}^a Department of Chemistry, The University of Western Ontario, London N6A 5B7, Canada^b Swedish Nuclear Fuel and Waste Management Company (SKB), Solna SE-169 03, Sweden^c Surface Science Western, The University of Western Ontario, London N6G 0J3, Canada^d Nuclear Waste Management Organization, Toronto M4T 2S3, Canada

ARTICLE INFO

Article history:

Received 10 August 2020

Revised 5 September 2020

Accepted 7 September 2020

Available online 15 September 2020

Keywords:

Copper

Sulfide

Cyclic voltammetry

Film

Pitting corrosion

Nuclear waste disposal

ABSTRACT

The formation of sulfide and oxide films on copper has been studied in sulfide solutions containing chloride and buffered to pH = 9 with borate over the temperature range 20 °C to 80 °C. The primary goal was to investigate the susceptibility of copper to pitting corrosion over a range of temperatures expected in a deep geological repository. Films were formed electrochemically and characterized using scanning electron microscopy (SEM), energy dispersive X-ray and Raman spectroscopy and X-ray diffractometry (XRD). Chalcocite (Cu₂S) formation was observed to occur under partially transport-controlled conditions in the potential range -0.9 V to -0.3 V vs SCE. At less negative potentials (≥ -0.3 V vs SCE), a transition from active dissolution to partial passivation by a copper oxide film was observed. Temperature had only a minor effect on the formation of the sulfide film, but the onset of active dissolution and oxide film formation shifted to lower potentials as the temperature increased.

© 2020 The Author(s). Published by Elsevier Ltd.

This is an open access article under the CC BY-NC-ND license

(<http://creativecommons.org/licenses/by-nc-nd/4.0/>)

1. Introduction

The internationally accepted method for the permanent disposal of high-level nuclear waste involves sealing it in corrosion-resistant containers to be subsequently emplaced in deep geologic repositories (DGR). In Sweden, Finland and Canada, the spent fuel would be sealed in containers fabricated with either a cast iron insert and a copper (Cu) shell (Sweden, Finland), or a carbon steel vessel with a Cu coating (Canada). Such containers would provide the only absolute barrier in a multi-barrier system designed to prevent radionuclide release to the environment [1–6]. The choice of Cu as the corrosion barrier is based on its corrosion resistance in the anoxic environments anticipated in a DGR [7,8], in which exposure conditions will evolve from initially warm (~ 90 °C) and oxidizing to eventually cool (~ 15°C) and anoxic [9]. The period required for the evolution in redox conditions to occur is uncertain [10] with recent field studies suggesting consumption of O₂, trapped on sealing the DGR, may be complete within the first 10 to 100 years after container emplacement in the DGR [11]. By con-

trast, the evolution in temperature, which can be controlled to a large extent by container and DGR design, is more readily calculated, and expected to evolve from a high of 80–90 °C during the first 100–200 years of emplacement to ~ 20 °C after several thousands of years [12]. Based on Swedish DGR design and calculations, containers are expected to remain uncompromised by corrosion for periods exceeding 10⁵ years with most containers surviving for > 10⁶ years [3,13,14].

While resistant to corrosion under anoxic conditions [7,10], copper is unstable in the presence of sulfide (S²⁻) or hydrosulfide (SH⁻) ions [10,15]. In a DGR, the production of SH⁻ is likely via the action of sulfate-reducing bacteria (SRB) [8] at locations remote from the Cu container surface. While SH⁻ transport to the Cu surface will be extremely slow [16] due to the high compaction density of the clay surrounding the container, corrosion induced by SH⁻ should be investigated.

A series of corrosion studies have shown that under anoxic conditions the corrosion of Cu in aqueous SH⁻ environments leads to the formation of chalcocite (Cu₂S) films on the Cu surface [10,15,17–19]. The properties of these films were found to depend on [SH⁻] and [Cl⁻] and their ratio, with Cl⁻ being one of the dominant groundwater anions. These studies showed that, while the growth law may change, these films remained

* Corresponding author at: Department of Chemistry, The University of Western Ontario, London N6A 5B7, Canada.

E-mail addresses: jchen496@uwo.ca (J. Chen), jjnoel@uwo.ca (J.J. Noël).

porous and only partially protective. Based on these studies, corrosion would be expected to propagate relatively uniformly in Swedish/Finnish/Canadian repositories, since the interfacial reaction of SH^- with Cu is rapid compared to SH^- transport via the compacted clay under SH^- transport-controlled conditions [20,21].

Other authors have claimed, however, that the film is passive in nature when formed under electrochemical conditions. Since passivity is a prerequisite for pitting corrosion, this would render the metal susceptible [22,23]. For instance, Dong et al. [22] measured the influence of temperature on supposedly pitting breakdown potentials in borate ($\text{HBO}_3^{2-}/\text{BO}_3^{3-}$) buffered, slightly alkaline solutions containing various $[\text{Cl}^-]$ and $[\text{SH}^-]$, and proposed that Cu would be susceptible to passivity and pitting under DGR conditions [22,23]. However, Martino et al. [24], based on electrochemical experiments conducted at room temperature in solutions containing various $[\text{SH}^-]$ and $[\text{Cl}^-]$, found film properties to be dependent on these concentrations and the flux of SH^- , controlled by the use of a rotating disk electrode [24]. They categorized the films according to their properties and demonstrated that only films formed in solutions containing $\geq 5 \times 10^{-4}$ M SH^- could be considered partially passive, and only when a high SH^- flux to the Cu surface was maintained. More recent studies, however, showed that, even at high $[\text{SH}^-]$, films formed anodically remained porous rather than becoming passive [25]. Sulfide concentrations are expected to be well below 10^{-4} M in Swedish and Finnish DGRs [3,10], and $< 10^{-6}$ M in a Canadian DGR [10]. This, coupled with the extremely low flux of SH^- through compacted clay, would reduce the surface $[\text{SH}^-]$ to a very low value [16]. These studies and calculations indicate that passivity, a prerequisite for pitting corrosion, should not be possible. However, the corrosion behavior of Cu in SH^- solutions is also influenced by the presence of other anions (SO_4^{2-} as well as Cl^-) [26], suggesting that the presence of $\text{HBO}_3^{2-}/\text{BO}_3^{3-}$ in the experiments of Dong et al. [21] and Kong et al. [27,28] could have influenced the properties of the Cu_2S films.

In a previous paper, we re-evaluated the formation of sulfide and oxide films on Cu under electrochemical conditions in $\text{HBO}_3^{2-}/\text{BO}_3^{3-}$ -containing solutions that either contained or were free of SH^- and various concentrations of chloride [29]. This published study demonstrated that $\text{HBO}_3^{2-}/\text{BO}_3^{3-}$ could induce passivity, but only in the potential range where oxide formation was thermodynamically possible, which is a potential that is much more positive than that at which Cu_2S formation occurred. In this study, we report results and analyses obtained under similar conditions as a function of temperature over the range from 20 to 80°C.

2. Experimental

2.1. Sample preparation

Copper samples used in all the experiments were oxygen-free and phosphorus-doped (30–100 wt.ppm), provided by the Swedish Nuclear Fuel and Waste Management Co (SKB), Solna, Sweden. Copper specimens for rotating disk electrodes (RDE) were machined with a threaded connection to a titanium (Ti) rod and sealed into a Teflon holder using epoxy resin. A non-conductive lacquer was applied to prevent exposure of the Ti/Cu junction to the electrolyte, leaving a flat Cu surface with a total surface area of 0.785 cm² exposed to the electrolyte. The average grain size of SKB Cu is ~150 μm [30,31]. Prior to each experiment, the Cu electrode was ground with a sequence of SiC papers with grit sizes: 800, 1000, 1200, 2400, 4000, and then polished to a mirror surface finish using aluminum oxide (Al_2O_3) suspensions with decreasing particle size (1 μm, 0.3 μm, and 0.05 μm), sonicated in methanol (reagent-grade) for 1 min, and finally dried in a stream of ultrapure (99.999%) Ar gas.

2.2. Electrochemical cell and instrumentation

Experiments were performed in a three-electrode cell using a Cu RDE working electrode, a Pt plate counter electrode, and a saturated calomel reference electrode (SCE, +0.242 V vs SHE). The cell was fitted with an outer glass jacket through which H₂O was circulated from a thermostatic bath (Isotemp 3016H Fisher Scientific) to maintain the temperature of the solution constant to within ± 1 °C. The electrochemical cell was placed inside a Faraday cage to reduce interference from external electrical noise. The RDE rotation rate (ω) was controlled by a Pine Instrument Company Analytical Rotator Model AFA86 Serial 882. Cyclic voltammograms (CV) were recorded using either a Solartron 1287 potentiostat or a Solartron Analytical Modulab equipped with CorrWare and XM-Studio-ECS software. Prior to each experiment, the electrode was cathodically cleaned at –1.5 V vs SCE for 1 min to reduce any air-formed oxides, and then at –1.15 V vs SCE for another minute to allow the detachment of any H₂ bubbles which may have formed due to H₂O reduction at the more negative potential. CVs and potential scans were performed from an initial potential of –1.35 V vs SCE to various anodic limits at a scan rate of 2 mV/s. Potentiostatic polarizations were conducted at –0.13 V vs SCE for 6 h at 33 Hz (80 °C).

2.3. Electrolyte and environment

Solutions were prepared with reagent-grade sodium chloride (NaCl, 99.0% assay), sodium sulfide ($\text{Na}_2\text{S}\cdot 9\text{H}_2\text{O}$, 98.0% assay), boric acid (H_3BO_3 , 99.5% assay), sodium borate decahydrate ($\text{Na}_2\text{B}_4\text{O}_7\cdot 10\text{H}_2\text{O}$, 99.5% assay) and Type I water (18.2 MΩ•cm) purified using a Barnstead NANOPure 7143 ultra pure water system. Electrodes were exposed to solutions containing 2×10^{-4} M SH^- (buffered with 0.2 M $\text{HBO}_3^{2-}/\text{BO}_3^{3-}$ to pH 9) and various chloride concentrations in the range from 0.01 M to 5 M. To ensure the maintenance of a deaerated environment and minimize sulfide oxidation, the solution was sparged with ultrapure Ar for 30 min prior to each experiment and then continuously throughout the experiment. The solution temperature was maintained by circulating H₂O from a thermostatic bath (Isotemp 3016H Fisher Scientific) with adjustable temperature control through a water jacket surrounding the cell. Experiments were performed at various temperatures, ranging from 20 to 80 °C (± 2 °C).

2.4. Surface analysis

Scanning electron microscopy (SEM) analyses were conducted using a LEO 1540 instrument equipped with a focused ion beam (FIB) (Zeiss Nano Technology System, Germany) at the Western Nanofabrication Facility. An electron beam with an accelerating voltage ranging between 1 kV and 5 kV was used to collect high-resolution images of both film morphologies and milled samples at various magnifications. Elemental compositions of sample surfaces were analysed using an energy dispersive X-ray spectrometer (EDX) in conjunction with the LEO 1540 FIB/SEM microscope and a Hitachi SU8230 Regulus Ultra High-Resolution Field Emission SEM coupled with a Bruker X-Flash EDX detector.

Raman spectroscopy was performed using a Renishaw InVia Reflex Raman spectrometer equipped with a 633 nm He-Ne laser and an Olympus microscope. Spectra were obtained using a 50 × uncoated objective lens with a laser beam diameter of ~ 2 μm. To minimize any surface heating effects, the laser beam was used at 1–5% power. Prior to the acquisition of spectra, the spectrometer was calibrated against the 520.5 cm⁻¹ peak of Si.

A Rigaku SmartLab X-ray diffractometer with Cu K α radiation (40 kV, 44 mA) was used to examine the phase composition of the surface film. The sample was scanned over a 2 θ range from 20°

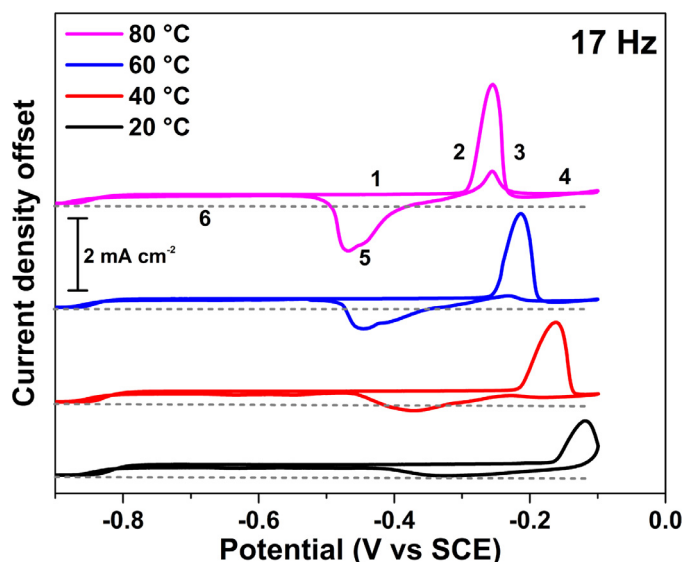


Fig. 1. CVs recorded in solution containing 0.1 M NaCl + 2×10^{-4} M Na₂S + 0.2 M borate (pH 9) at $\omega = 17$ Hz and at various temperatures. The numbers 1–6 refer to different regions.

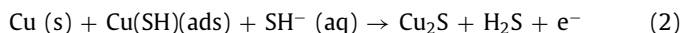
to 95° with a 0.02° step size. A grazing incidence angle configuration (GIXRD) with an incidence angle of 2.5° was used to minimize interference from the Cu substrate.

3. Results and discussion

3.1. Borate-buffered solutions containing sulfide and chloride at various temperatures

A series of CVs were recorded from -1.35 V to -0.1 V vs SCE in a solution containing 0.1 M NaCl + 2×10^{-4} M Na₂S + 0.2 M HBO₃²⁻/BO₃³⁻ (pH = 9). Fig. 1 shows the sections of the CVs from -0.9 V to -0.1 V vs SCE at various temperatures. In Fig. 2, two sections of the scans conducted at 80 °C and various electrode rotation rates (ω) are shown: (a) -0.9 V to -0.1 V vs SCE; and (b) -1.25 V to -0.85 V vs SCE. As indicated in these figures, a number of specific regions can be defined.

The current in region 1 has been demonstrated [24,29] to be due to the anodic formation of chalcocite (Cu₂S), reactions (1) and (2), with the formation of oxide/hydroxide and soluble Cu complexes prohibited in this potential range [7].



The current in region 1 was independent of potential (E), Fig. 1, but increased with ω , Fig. 2 (a). In addition, although not shown here, the current was maintained on the reverse scan if the potential scan was reversed at other potentials in this region, which was consistent with previous results recorded at 20 °C [24]. This set of observations would only be possible if the Cu₂S film formed on the forward scan was porous, and its formation was at least partially transport-controlled and sustained on the reverse scan. If the film formed on the forward scan had been passive, the current on the reverse scan would have been effectively zero since the electric field within such a film would have been too low to sustain the further film growth observed. A significant increase in current was observed when the scan was extended into region 2, where dissolution as CuCl_x^{(x-1)-} became possible. The shift of the current increase in region 2 to lower potentials as the temperature

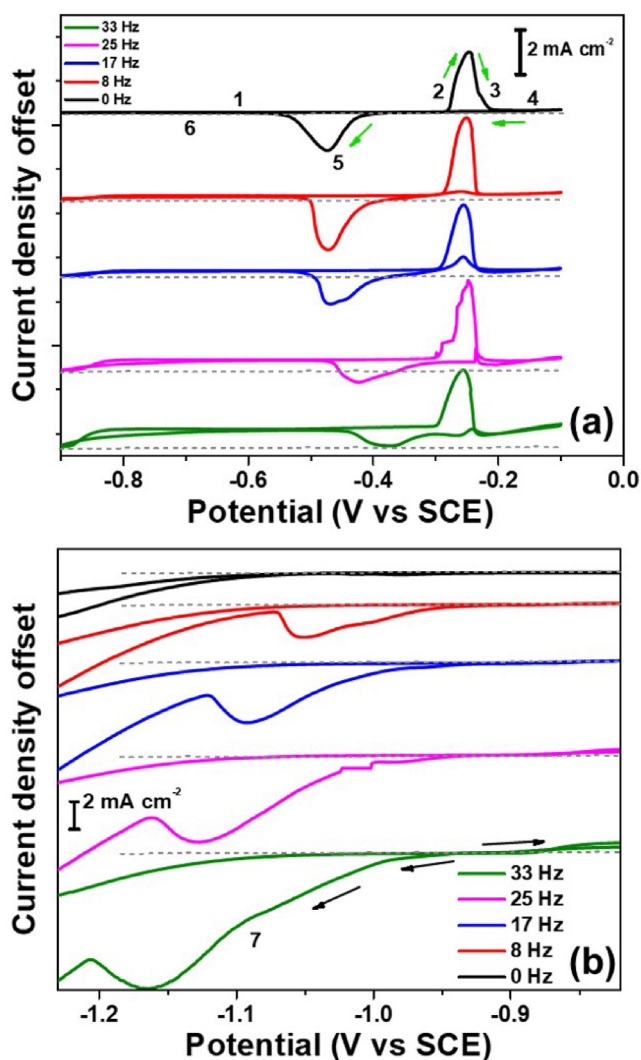
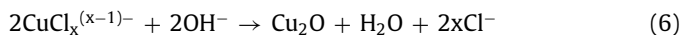
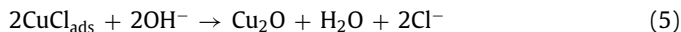
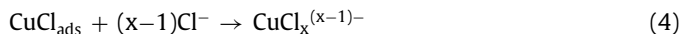


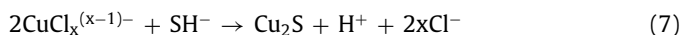
Fig. 2. CVs conducted in solutions containing 0.1 M NaCl + 2×10^{-4} M Na₂S + 0.2 M borate (pH 9) at 80 °C at various values of the electrode rotation rate (ω). (a) shows the section of the scans between -0.9 V to -0.1 V vs SCE; (b) shows the sections of the same scans between -1.25 V and -0.83 V vs SCE.

was increased suggested a significant influence of temperature on this anodic dissolution step. Since anion adsorption on Cu is well known to occur, this could suggest a preference for increased Cl⁻ adsorption at the higher temperatures. The subsequent decrease in current in region 3 suggested an active-to-passive transition which shifted to lower potentials as the temperature was increased. The current in region 2 was only slightly dependent on ω , while the decrease in region 3 was independent of ω , Fig. 2 (a). This was also similar to the behavior observed at 20 °C [24]. Since we demonstrated previously that such current increases were observed in the absence of SH⁻, they can be attributed to the anodic dissolution of Cu, with a minor dependence on ω , and thus less dependent on the transport of chloride ions, due to the occurrence of these reactions within the pores of the Cu₂S layer formed at lower potentials (≤ -0.3 V vs SCE). The reactions occurring in this potential range have been extensively studied [8,32]. The rapid decrease in current in region 3 was shown, at room temperature, to be due to the formation of a Cu₂O/CuO layer induced by the presence of HBO₃²⁻/BO₃³⁻ (at pH 9) irrespective of whether SH⁻ was present. Oxide formation could proceed directly by oxidation of the Cu surface or by the hydrolysis of the surface layer formed in reaction (3)–(5), or of dissolved CuCl_x^{(x-1)-}, reaction (6) [32,33].



The low current in region 4, Fig. 1, suggested the formation of a passive oxide film. However, the increase in current (region 4) with temperature, Fig. 1, and ω , Fig. 2 (a), and the recovery of the current for anodic dissolution (as $\text{CuCl}_x^{(x-1)-}$) in regions 2 and 3 on the return scan confirmed that passivation was incomplete, especially for $T \geq 60$ °C. The cathodic reduction peak in region 5, Figs. 1 and 2 (a), can be attributed to the reduction of the anodically-formed oxides and $\text{CuCl}_x^{(x-1)-}$ trapped within the pores of the Cu_2S film. This was consistent with the observation that the anodic charge increased in regions 2 and 4 as temperature increased, Fig. 1. The charge associated with reduction peak 5 also increased as expected.

Fig. 2 (a) shows that, at a stationary electrode ($\omega = 0$ Hz), the cathodic charge recovered in region 5 was close to that consumed by anodic oxidation in regions 2 and 3, which was consistent with the retention at the electrode surface of the majority of the anodic products, which could then be reduced on the reverse scan. When ω was increased, the charge associated with region 5 decreased and, for a sufficiently high value of ω , the net current in this region became positive, Fig. 2 (a), suggesting a net oxidation process. This can be attributed to a combination of the increased fluxes of reducible $\text{CuCl}_x^{(x-1)-}$ away from the electrode surface, which prevented its cathodic reduction, and of SH^- into the porous structure, which led to the enhanced anodic formation of Cu_2S , with the current becoming positive when the anodic process became dominant at high values of ω . The combination of these two fluxes would also be expected to lead to the rapid chemical deposition of Cu_2S on the Cu surface via the chemical reaction (7) [34], with the Cu_2S not being able to be reduced until the potential was scanned to region 7. Additionally, an increased flux of SH^- to the Cu surface would also lead to the chemical conversion from Cu_2O to Cu_2S , although this reaction is not particularly fast compared to reaction 7 [35].



The revival of the current for the anodic formation of Cu_2S in region 6 on the reverse scan, Figs. 1 and 2 (a), confirmed that the Cu_2S film formed on the forward scan remained porous and continued to grow. The recovery of the current observed in region 6 to that observed in region 1 on the forward scan was almost complete, especially at the higher temperatures, Fig. 1, indicating that the film formation/reduction processes at higher potentials had only a minor influence on the anodic formation of Cu_2S . Fig. 2 (b) shows the cathodic reduction peaks of Cu_2S in region 7. Commonly, two reduction peaks are observed in this region [24], reflecting the distinct morphologies of these films. Previously, it has been shown that the cathodic charge associated with Cu_2S reduction (Q_C) was approximately equal to the anodic charge (Q_A) consumed in its formation. In this study, while Q_C increased as Q_A increased, it was difficult to perform a quantitative comparison due to the large partially overlapping current for H_2O reduction which accounted for the rapidly increasing current at more negative potentials ($E \leq -1.1$ V vs SCE), Fig. 2 (b). The significant increase in current associated with H_2O reduction reaction ($E \leq -1.1$ V vs SCE) could be attributed to an increase in total surface area of the Cu particulates formed during the cathodic reduction of Cu_2S .

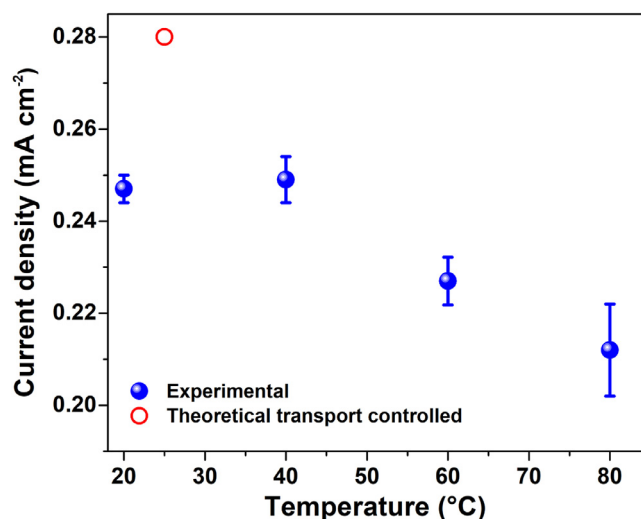


Fig. 3. Limiting current densities at $E = -0.6$ V vs SCE plotted as a function of solution temperature taken from the CVs in Fig. 1. The red open circle shows the current density for theoretical transport-control at 25 °C. (For interpretation of the references to color in this figure legend, the reader is referred to the web version of this article.)

3.2. The influence of temperature on sulfide film formation

Fig. 3 shows the current densities recorded at $E = -0.6$ V vs SCE (i.e., in region 1) in CV experiments and at $\omega = 17$ Hz for all the temperatures studied. Similar behavior was observed at other values of ω ranging from 8 Hz to 33 Hz. At all temperatures, the current densities were substantially lower than the theoretical transport-limited current, as indicated by the red circle which was calculated at 25 °C using the Levich equation [36]. While the measured current density decreased only slightly with temperature, the deviation from transport control was greater at the higher temperatures, since the theoretical transport-limiting current would have increased with increasing temperature. This influence of temperature on the potential-independent current in region 1 was contrary to that claimed by others [22,28] who observed a slight increase. This slight increase was attributed by those authors to an increase in generation of cation vacancies as the temperature was increased, and the condensation of cation vacancies at the metal/barrier layer interface was considered to account for the passive film breakdown [22,27,28].

3.3. The influence of temperature on chloride-induced active dissolution and oxide formation

The potential at which the current began to rise in region 2, Fig. 1, can be defined as the onset potential at which the anodic oxidation associated with the formation of soluble $\text{CuCl}_x^{(x-1)-}$ species began. This potential was determined by plotting the current logarithmically and defining the onset potential as the intersection of the extrapolated currents in regions 1 and 2, as shown in Fig. 4. These onset potentials, and similar values obtained at different concentrations of Cl^- over the range from 0.1 M to 5.0 M, are plotted for three temperatures (40, 60 and 80 °C) in Fig. 5. Included in this plot are the potentials which Dong et al. [22] claimed were Cl^- -induced breakdown potentials for the Cu_2S films grown at lower potentials in region 1, Fig. 2. The similarity between the two sets of data demonstrates that the values measured by Dong et al. [22] represented onset potentials for anodic dissolution, not Cu_2S film breakdown values.

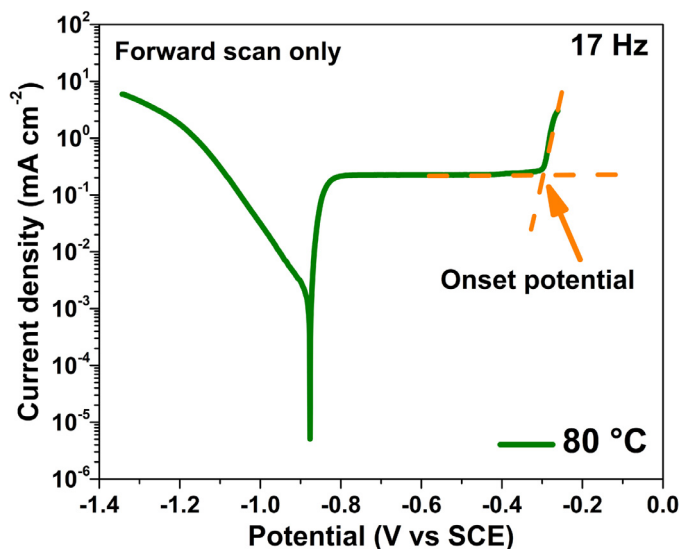


Fig. 4. Potentiodynamic polarization conducted on copper in a 0.1 M NaCl + 2×10^{-4} M Na₂S + 0.2 M borate (pH 9) solution at 80 °C and at the electrode rotation rate (ω) of 17 Hz. The onset potential is indicated by the intersection between horizontal line for zero current density and the tangent to the increasing current.

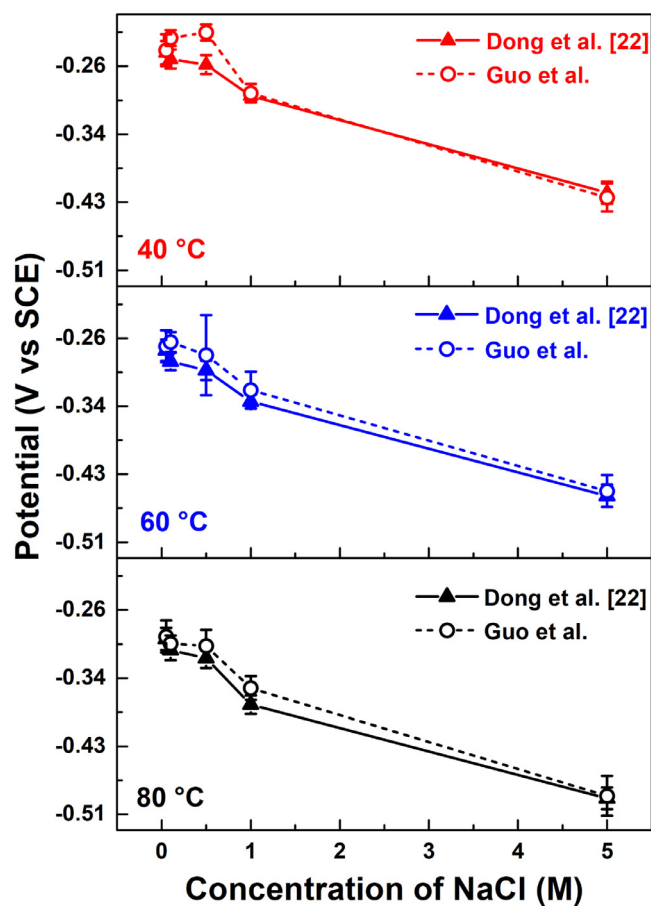


Fig. 5. Comparison of the potentials at which the current increases in CVs (Fig. 1) to those measured by others and claimed to be sulfide film breakdown potentials.

3.4. Characterizations of electrochemically grown films

SEM micrographs recorded on the surfaces of electrodes after scanning the potential to various potential limits at $\omega = 33$ Hz at a temperature of 80 °C are shown in Fig. 6. FIB-cut cross-sections of these electrodes are shown in Fig. 7. When the potential limit was -0.85 V vs SCE (i.e., confined to the early section of region 1), the SEM micrograph in Fig. 6 (a) showed the formation of only a thin film, and the grinding ridges from surface preparation remained visible. The extremely small apparent pit-like features occur at the locations where SiC and Al₂O₃ particles were embedded in the soft metal surface during electrode preparation, as demonstrated by EDX. The cross-section in Fig. 7 (a) shows that the Cu₂S film was thin and porous, with a maximum thickness of 367 nm, but with many locations where the film was considerably thinner. This approximate maximum thickness was considerably larger than that for the film grown under similar conditions at 20 °C (≤ 150 nm) [29], despite the observation that the plateau current in region 1 was smaller at 80 °C than at 20 °C, Fig. 4. As a consequence, the overall extent of film formation would be expected to be lower at the higher temperature, leading to a correspondingly thinner film if the thickness was determined by charge only. The FIB-cut cross-sectional image in Fig. 7 (a) shows that the film grown at 80 °C was composed of columnar features that were non-uniformly distributed on the surface. This columnar growth at the higher temperature could be attributed to the more extensive transport of Cu species than that at the lower temperature. As shown previously, Cu₂S film growth occurred at the film/solution interface, with transport occurring in the form of either Cu(SH)₂⁻ complexes or Cu₃S₃ clusters [34]. When the potential was scanned to $E = -0.4$ V vs SCE, a scattered dendritic Cu₂S deposit was formed on top of a fine particulate base layer, Fig. 6 (b). The cross-section shown in Fig. 7 (b) revealed that the particulate base layer, while apparently more compact and evenly distributed, remained porous and continued to grow in a columnar manner. While the Cu surface was slightly rougher, there was no indication of pitted locations at the Cu/film interface. One particularly long columnar feature is marked in Fig. 7 (b).

When the potential scan limit was extended to -0.24 V vs SCE and eventually to -0.13 V vs SCE, the outer dendritic became denser, and achieved an apparent thickness of 5 μ m but contained extensive void spaces, Fig. 6 (c) and (d). The porous particulate base layer reached a thickness of 280 nm to 398 nm at -0.24 V vs SCE and did not thicken noticeably when the potential was extended to -0.13 V vs SCE, Fig. 7 (c) and (d). This base layer maintained its coherence at -0.24 V vs SCE, a potential in region 3 at 80 °C, and the Cu surface showed no indication of pitting. At -0.13 V vs SCE, when the CV in Fig. 2 (at 80 °C) indicated a partially passive state (region 4), the base layer appeared to have broken up slightly, Fig. 7 (d).

Raman spectra were collected at various surface locations after the potential was scanned to -0.4 V vs SCE (region 1) and -0.13 V vs SCE (region 4), Fig. 8. The spectrum recorded at -0.4 V vs SCE showed a broad peak at 297 cm⁻¹, confirming the presence of Cu₂S [35,37–39]. The very shallow response in the wavenumber range 500 cm⁻¹ to 625 cm⁻¹ may indicate slight conversion of the Cu₂S to oxide by reaction with air, which can be attributed to the local heating effect induced by the laser beam while the spectrum was recorded [40,41]. In the spectrum recorded at -0.13 V vs SCE, the peak at 297 cm⁻¹ could be due to either Cu₂S or CuO, since the formation of the latter was also thermodynamically possible at this potential [7]. The peaks at 147 cm⁻¹ and 220 cm⁻¹, and the less well-defined peaks in the range 500 cm⁻¹ to 625 cm⁻¹ confirm the presence of Cu₂O [42]. To confirm these compositions, grazing incidence X-ray diffraction patterns were recorded after 6 h of potentiostatic oxidation at -0.13 V vs SCE at 80 °C, Fig. 9. Comparison

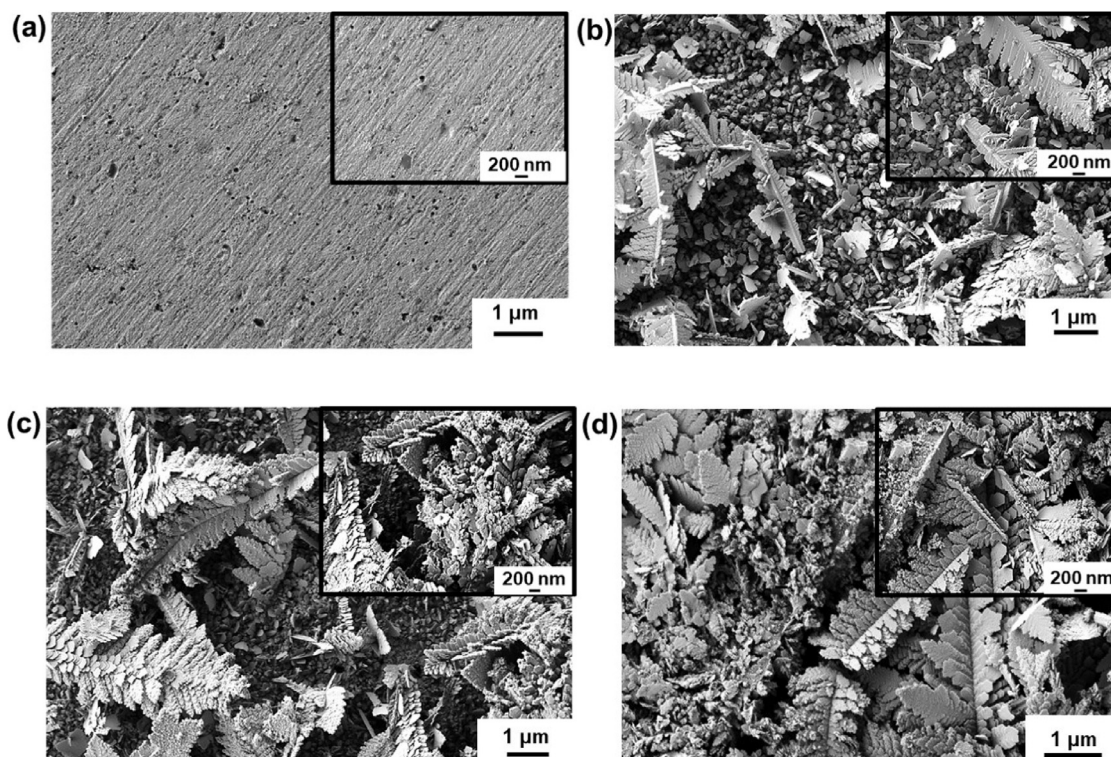


Fig. 6. SEM micrographs showing morphologies of films formed after scanning potential to various limits at 80 °C in solutions containing 0.1 M NaCl + 2×10^{-4} M Na₂S + 0.2 M borate. (a) -0.85 V vs SCE, (b) -0.40 V vs SCE, and (c) -0.24 V vs SCE, (d) -0.13 V vs SCE.

to standards confirmed the presence of Cu₂S and Cu₂O but did not detect CuO.

Fig. 10 shows EDX elemental maps (expressed as wt.%) recorded on a mechanically polished cross-section of the Cu electrode anodically oxidized at -0.13 V vs SCE for 6 h (80 °C). The high Si and O wt.% at the top of the maps indicate the locations of the epoxy resin used to protect the surface layers during cutting and polishing of the cross-section. The void space throughout the film, observed in the SEM/FIB micrographs, Fig. 7, was also evident in the maps for Cu, O and S, shown in Fig. 10. Sulfur was mostly detected on the top, while the majority of the O associated with oxide was located in the middle of the film and at the Cu/film interface. The body of the film was mainly composed of copper oxide (Cu₂O, as indicated the by XRD analysis) with islands of Cu metal distributed in the oxide (red spots in Fig. 10(b)) attributable to Cu particles produced during the mechanical polishing.

At the Cu/film interface, the surface layer contained some Cu₂S, but was predominantly oxide, consistent with the dominant formation of a partially protective oxide at $E = -0.13$ V vs SCE, as suggested by the electrochemical results, Fig. 2 (a). While Cu₂S formation at the Cu/film interface was limited, a thick layer of Cu₂S was formed at the film/solution interface (i.e., at the film/epoxy interface in the maps) with only relatively small amounts present in the thick, void-filled body of the film. Since the anodic reaction of Cu with SH⁻ is rapid, limited film growth on the Cu surface can be attributed to SH⁻ depletion at this location, the surface [SH⁻] being controlled by transport through the thick film. The accumulation of a much thicker Cu₂S layer at the film/solution interface would be expected when the anodically-formed CuCl_x^{(x-1)-} was transported through pores within the film to the film/solution interface to react with SH⁻, via Reaction 7, on encountering the bulk [SH⁻], leading to the deposition of Cu₂S.

4. Conclusions

- 1) The kinetics of electrochemically-grown chalcocite (Cu₂S) films on Cu in the potential range -0.8 V vs SCE to -0.3 V vs SCE were partially transport-controlled and developed a porous, non-passive structure. Temperature had only a minor influence on the kinetics of film growth.
- 2) At more positive potentials (≥ -0.3 V vs SCE) an active to passive transition was observed, with active dissolution occurring as CuCl_x^{(x-1)-} within the Cu₂S film formed at lower potentials, followed by the partial passivation of the surface by the formation of Cu₂O. The potential range within which these two processes occurred decreased as the temperature increased.
- 3) The potentials at which active dissolution commenced coincided with the potentials erroneously claimed in the literature to be chloride-induced sulfide film breakdown potentials. This coincidence of values was observed at all temperatures studied in the range 20 to 80 °C.
- 4) Raman spectroscopy and XRD confirmed the formation of chalcocite (Cu₂S) in the low potential region ($E = -0.4$ V vs SCE) and Cu₂S/Cu₂O at higher potentials ($E \geq -0.3$ V vs SCE).
- 5) SEM micrographs and EDX analyses confirmed the presence of oxides at the Cu/film interface covered by a thick extremely porous overlayer with a thick deposited outer layer of Cu₂S formed by the reaction of SH⁻ with CuCl_x^{(x-1)-} transported from the Cu surface.

Declaration of Competing Interest

The authors declare that they have no known competing financial interests or personal relationships that could have appeared to influence the work reported in this paper.

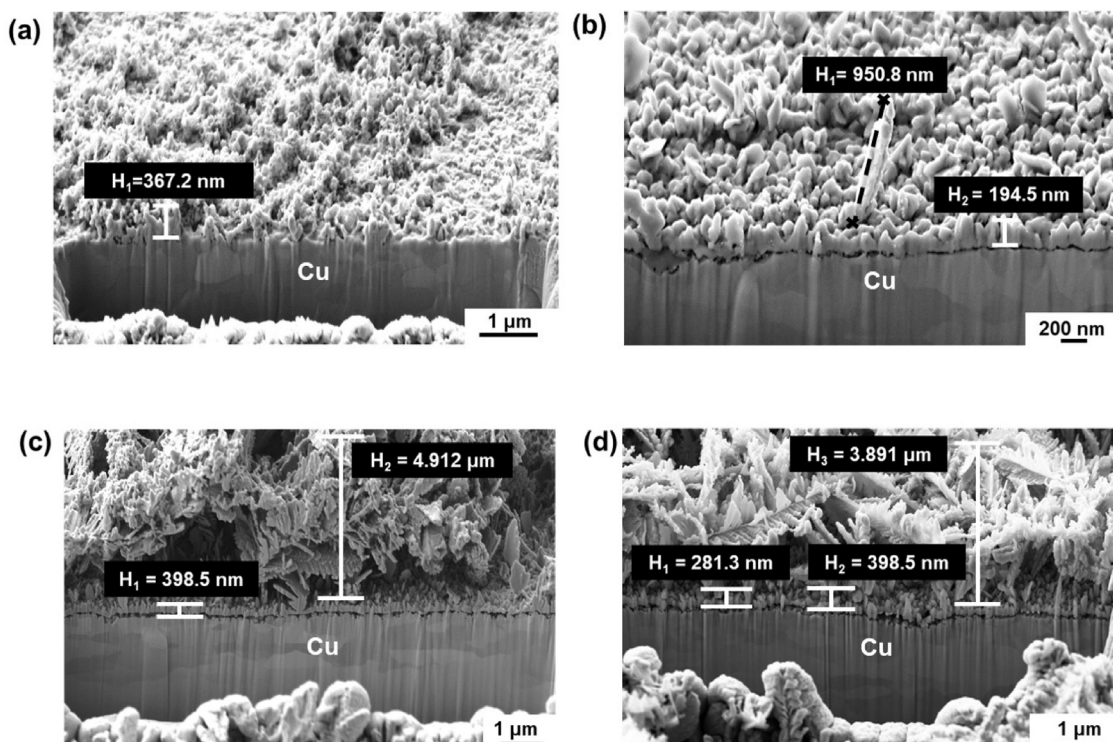


Fig. 7. FIB cut cross-sections of films formed after scanning potential to various limits 80 °C in solutions containing 0.1 M NaCl + 2×10^{-4} M Na₂S + 0.2 M borate (pH 9). (a) -0.85 V vs SCE, (b) -0.40 V vs SCE, and (c) -0.24 V vs SCE, (d) -0.13 V vs SCE.

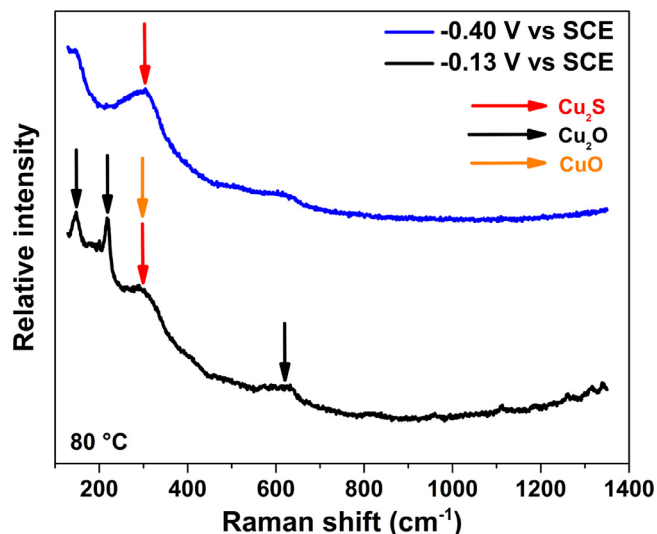


Fig. 8. Raman spectra recorded on two Cu samples after potentiodynamic polarization. The potential was scanned from -1.35 V to different potentials (vs SCE) at the scan rate of 2 mV/s.

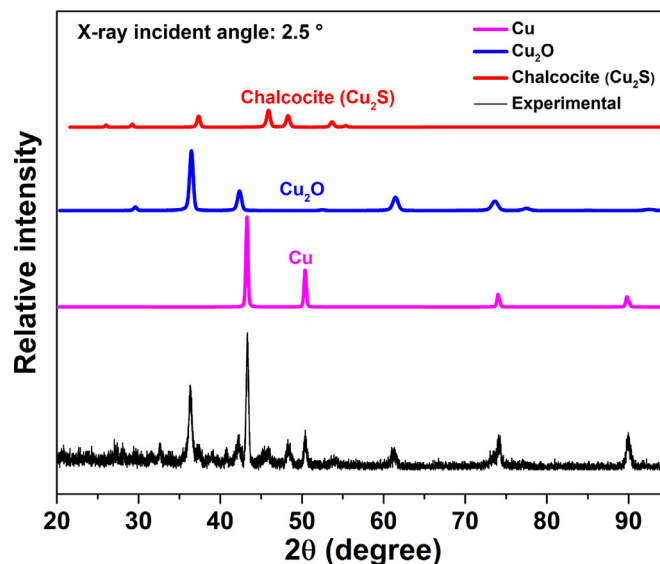


Fig. 9. Grazing incidence XRD patterns of a Cu sample after potentiostatic polarization at -0.13 V vs SCE in a solution containing 0.1 M NaCl + 2×10^{-4} M Na₂S + 0.2 M borate (pH 9) for 6 h at 80 °C, together with standards obtained from the Rigaku SmartLab XRD database.

CRediT authorship contribution statement

M. Guo: Methodology, Validation, Formal analysis, Investigation, Data curation, Writing - original draft, Writing - review & editing, Visualization. **J. Chen:** Methodology, Formal analysis, Investigation, Writing - review & editing. **C. Lilja:** Resources, Writing - review & editing, Project administration, Funding acquisition. **V. Dehnavi:** Methodology, Formal analysis, Investigation. **M. Behazin:** Resources, Writing - review & editing, Project administration, Funding acquisition. **J.J. Noël:** Conceptualization, Methodol-

ogy, Formal analysis, Resources, Writing - review & editing, Supervision, Project administration, Funding acquisition.

Acknowledgment

This research was funded by the Swedish Nuclear Fuel and Waste Management Company (SKB, Solna, Sweden) and the Nuclear Waste Management Organization (Toronto, Canada) and the Natural Sciences and Engineering Research Council of Canada

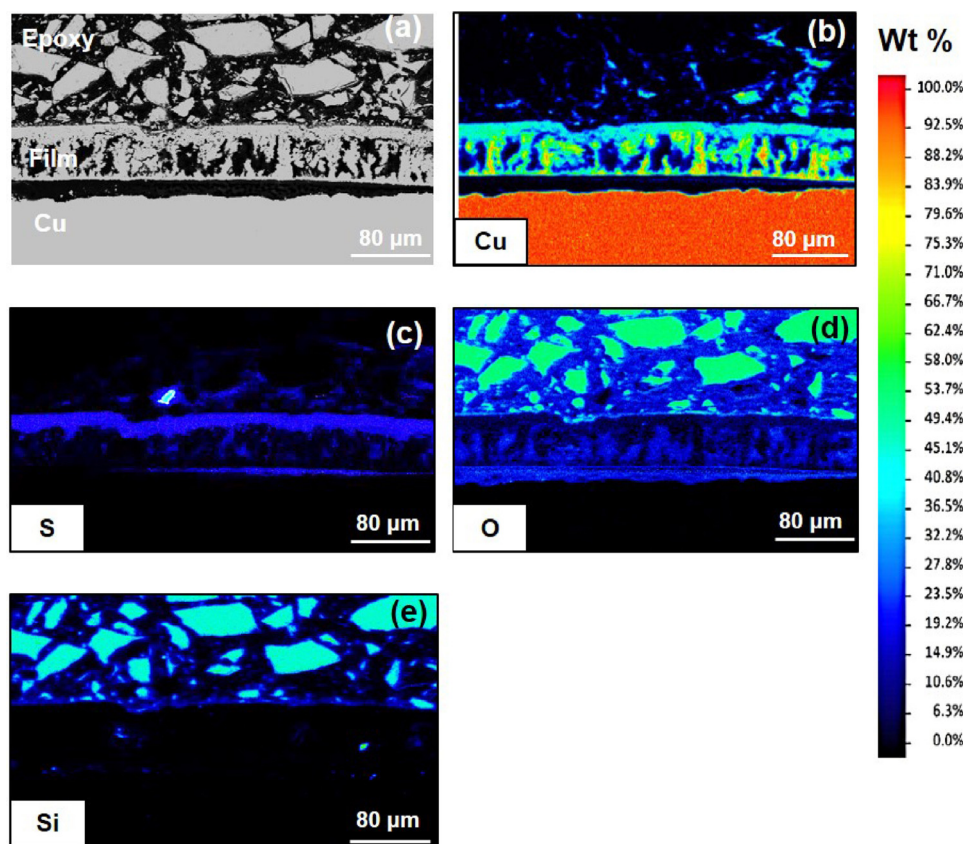


Fig. 10. SEM micrograph and respective EDX weight percentage elemental maps of the cross-sections of an anodic film grown after potentiostatic polarization at -0.13 V vs SCE in solutions containing 0.1 M NaCl + 2×10^{-4} M Na₂S + 0.2 M borate (pH 9) for 6 h at 80°C . (For interpretation of the images based on the color scale in this figure, the reader is referred to the web version of this article.)

(NSERC) under a Collaborative Research and Development grant (CRDPJ 507465 – 16). The authors thank Mary Jane Walzak (Surface Science Western) and Todd Simpson (Western Nanofabrication Facility) for many useful discussions and assistance with laser Raman spectroscopy and SEM/FIB analyses.

References

- [1] D. Arcos, F. Grandia, C. Domènech, Geochemical Evolution of the Near Field of a KBS-3 Repository, Svensk Kärnbränslehantering AB, 2006 Technical Report, TR-06-16.
- [2] A. Hedin, Long-term Safety for KBS-3 Repositories at Forsmark and Laxemar – A First Evaluation. Main Report of the SR-Can project, Svensk Kärnbränslehantering AB, 2006 Technical Report, TR-06-09.
- [3] Long-term Safety for the Final Repository for Spent Nuclear Fuel at Forsmark – Main Report of the SR-Site project, Long-term Safety for the Final Repository for Spent Nuclear Fuel at Forsmark – Main Report of the SR-Site project, Svensk Kärnbränslehantering AB, 2011 Technical Report, TR-11-01.
- [4] P.G. Keech, P. Vo, S. Ramamurthy, J. Chen, R. Jacklin, D.W. Shoesmith, Design and development of copper coatings for long term storage of used nuclear fuel, *Corros. Eng. Sci. Technol.* 49 (2014) 425–430.
- [5] C.H. Boyle, S.A. Meguid, Mechanical performance of integrally bonded copper coatings for the long term disposal of used nuclear fuel, *Nucl. Eng. Des.* 293 (2015) 403–412.
- [6] D.S. Hall, P.G. Keech, An overview of the Canadian corrosion program for the long-term management of nuclear waste, *Corros. Eng. Sci. Technol.* 52 (2017) 2–5.
- [7] I. Puigdomenech, C. Taxén, Implications for the Corrosion of Copper Under Repository Conditions, Svensk Kärnbränslehantering AB, 2000 Technical Report, TR-00-13.
- [8] F. King, C. Lilja, K. Pedersen, P. Pitkänen, M. Vähänen, An Update of the State-of-the-Art Report on the Corrosion of Copper Under Expected Conditions in a Deep Geologic Repository, Svensk Kärnbränslehantering AB, 2010 Technical Report, TR-10-67.
- [9] T. Standish, J. Chen, R. Jacklin, P. Jakupi, S. Ramamurthy, D. Zagidulin, P. Keech, D. Shoesmith, Corrosion of copper-coated steel high level nuclear waste containers under permanent disposal conditions, *Electrochim. Acta* 211 (2016) 331–342.
- [10] F. King, D.S. Hall, P.G. Keech, Nature of the near-field environment in a deep geological repository and the implications for the corrosion behaviour of the container, *Corros. Eng. Sci. Technol.* 52 (2017) 25–30.
- [11] H. Müller, B. Garitte, T. Vogt, S. Köhler, T. Sakaki, H. Weber, T. Spillmann, M. Hertrich, J. Becker, N. Giroud, V. Cloet, N. Diomidis, T. Vietor, Implementation of the full-scale emplacement (FE) experiment at the Mont Terri rock laboratory, *Swiss J. Geosci.* 110 (2017) 287–306.
- [12] Supplementary Information on Canister Integrity Issues, Svensk Kärnbränslehantering AB, 2019 Technical Report, TR-19-15.
- [13] Long-term Safety for the Final Repository for Spent Nuclear Fuel at Forsmark Main report of the SR-Site Project, Long-term Safety for the Final Repository for Spent Nuclear Fuel at Forsmark Main report of the SR-Site Project, II, Svensk Kärnbränslehantering AB, 2011 Technical Report, TR-11-01.
- [14] Long-term Safety for the Final Repository for Spent Nuclear Fuel at Forsmark Main report of the SR-Site Project, Long-term Safety for the Final Repository for Spent Nuclear Fuel at Forsmark Main report of the SR-Site Project, III, Svensk Kärnbränslehantering AB, 2011 Technical Report, TR-11-01.
- [15] J. Chen, Z. Qin, D.W. Shoesmith, Rate controlling reactions for copper corrosion in anaerobic aqueous sulphide solutions, *Corros. Eng. Sci. Technol.* 46 (2011) 138–141.
- [16] F. King, J. Chen, Z. Qin, D. Shoesmith, C. Lilja, Sulphide-transport control of the corrosion of copper canisters, *Corros. Eng. Sci. Technol.* 52 (2017) 210–216.
- [17] J. Chen, Z. Qin, T. Martino, D.W. Shoesmith, Effect of chloride on Cu corrosion in anaerobic sulphide solutions, *Corros. Eng. Sci. Technol.* 52 (2017) 40–44.
- [18] J. Chen, Z. Qin, D.W. Shoesmith, Kinetics of corrosion film growth on copper in neutral chloride solutions containing small concentrations of sulfide, *J. Electrochem. Soc.* 157 (2010) C338–C345.
- [19] J. Chen, Z. Qin, D.W. Shoesmith, Long-term corrosion of copper in a dilute anaerobic sulfide solution, *Electrochim. Acta* 56 (2011) 7854–7861.
- [20] S. Briggs, J. McKelvie, P. Keech, B. Sleep, M. Krol, Transient modelling of sulphide diffusion under conditions typical of a deep geological repository, *Corros. Eng. Sci. Technol.* 52 (2017) 200–203.
- [21] E.P. Kremer, Durability of the Canadian used fuel container, *Corros. Eng. Sci. Technol.* 52 (2017) 173–177.
- [22] C. Dong, F. Mao, S. Gao, S. Sharifi-Asl, P. Lu, D.D. Macdonald, Passivity breakdown on copper: influence of temperature, *J. Electrochem. Soc.* 163 (2016) C707–C717.
- [23] F. Mao, C. Dong, S. Sharifi-Asl, P. Lu, D.D. Macdonald, Passivity breakdown on copper: influence of chloride ion, *Electrochim. Acta* 144 (2014) 391–399.
- [24] T. Martino, R. Partovi-Nia, J. Chen, Z. Qin, D.W. Shoesmith, Mechanisms of film

- growth on copper in aqueous solutions containing sulphide and chloride under voltammetric conditions, *Electrochim. Acta* 127 (2014) 439–447.
- [25] T. Martino, J. Chen, Z. Qin, D.W. Shoesmith, The kinetics of film growth and their influence on the susceptibility to pitting of copper in aqueous sulphide solutions, *Corros. Eng. Sci. Technol.* 52 (2017) 61–64.
- [26] T. Martino, J. Chen, J.J. Noël, D.W. Shoesmith, The effect of anions on the anodic formation of copper sulphide films on copper, *Electrochim. Acta* 331 (2019) 135319.
- [27] D. Kong, C. Dong, A. Xu, C. Man, C. He, X. Li, Effect of sulfide concentration on copper corrosion in anoxic chloride-containing solutions, *J. Mater. Eng. Perform.* 26 (2017) 1741–1750.
- [28] D. Kong, A. Xu, C. Dong, F. Mao, K. Xiao, X. Li, D.D. Macdonald, Electrochemical investigation and ab initio computation of passive film properties on copper in anaerobic sulphide solutions, *Corros. Sci.* 116 (2017) 34–43.
- [29] M. Guo, J. Chen, T. Martino, M. Biesinger, J.J. Noël, D.W. Shoesmith, The susceptibility of copper to pitting corrosion in borate-buffered aqueous solutions containing chloride and sulfide, *J. Electrochem. Soc.* 166 (2019) C550–C558.
- [30] H.C.M. Andersson-Östling, J. Hagström, M. Danielsson, Phosphorus in Copper Intended for Spent Nuclear Fuel Disposal, *Svensk Kärnbränslehantering AB*, 2018 Report, R-17-19.
- [31] R. Wu, J. Hagström, R. Sandström, Grain Boundary Sliding in Phosphorus Alloyed Oxygen-Free Copper Under Creep, *Svensk Kärnbränslehantering AB*, 2015 Report, R-15-14.
- [32] G. Kear, B.D. Barker, F.C. Walsh, Electrochemical corrosion of unalloyed copper in chloride media—a critical review, *Corros. Sci.* 46 (2004) 109–135.
- [33] F. King, Corrosion of Copper In Alkaline Chloride Environments, *Svensk Kärnbränslehantering AB*, 2002 Technical Report, TR-02-25.
- [34] J. Chen, Z. Qin, T. Martino, M. Guo, D.W. Shoesmith, Copper transport and sulphide sequestration during copper corrosion in anaerobic aqueous sulphide solutions, *Corros. Sci.* 131 (2018) 245–251.
- [35] J.M. Smith, J.C. Wren, M. Odziemkowski, D.W. Shoesmith, The electrochemical response of preoxidized copper in aqueous sulfide solutions, *J. Electrochem. Soc.* 154 (2007) C431–C438.
- [36] V.G. Levich, S. Technicothers, *Physicochemical Hydrodynamics*, Prentice-Hall, Englewood Cliffs, NJ, 1962.
- [37] A. Kudelski, Structures of monolayers formed from different HS–(CH₂)₂–X thiols on gold, silver and copper: comparative studies by surface-enhanced Raman scattering, *J. Raman Spectrosc.* 34 (2003) 853–862.
- [38] G. Parker, G.A. Hope, R. Woods, Raman spectroscopic identification of surface species in the leaching of chalcopyrite, *Colloids Surf. A* 318 (2008) 160–168.
- [39] R. Woods, G.A. Hope, K. Watling, A SERS spectroelectrochemical investigation of the interaction of 2-mercaptobenzothiazole with copper, silver and gold surfaces, *J. Appl. Electrochem.* 30 (2000) 1209–1222.
- [40] J.R. Mycroft, G.M. Bancroft, N.S. McIntyre, J.W. Lorimer, I.R. Hill, Detection of sulphur and polysulphides on electrochemically oxidized pyrite surfaces by X-ray photoelectron spectroscopy and Raman spectroscopy, *J. Electroanal. Chem. Interfacial Electrochem.* 292 (1990) 139–152.
- [41] Y. Huang, R. Field, Q. Chen, Y. Peng, M.S. Walczak, H. Zhao, G. Zhu, Z. Liu, L. Li, Laser induced molybdenum sulphide loading on doped graphene cathode for highly stable lithium sulphur battery, *Commun. Chem.* 2 (2019) 1–8.
- [42] M. Liu, J. Li, In-situ Raman characterization of initial corrosion behavior of copper in neutral 3.5%(wt.) NaCl solution, *Materials* 12 (2019) 2164.